LANGMUIR

pubs.acs.org/Langmuir Article

Radioluminescent Photonic Bandgap Hydrogels: Mechanochromic Tunable Emissions

Sarah Mell, Haley W. Jones, Yuriy P. Bandera, and Stephen H. Foulger*

Cite This: *Langmuir* 2022, 38, 10089−10097 Read Online

ACCESS | Metrics & More | Article Recommendations

ABSTRACT: Fully organic, radioluminescent crystalline colloidal arrays (CCAs) with covalently incorporated emitters were synthesized by using up to three organic fluorophores that were Förster resonance energy transfer (FRET) pairs with each other. The emitters were covalently incorporated into monodisperse poly(styrene-*co*-propargyl acrylate) nanoparticles in various combinations, resulting in blue-, green-, and red-emitting CCAs when excited with an X-ray source. The negatively charged surfaces of the monodisperse nanoparticles caused self-assembly into a crystal-like structure, which resulted in a partial photonic bandgap (i.e., rejection wavelength) within the near-visible and visible light spectrum. When the rejection wavelength of the CCA overlapped its radioluminescence, the spontaneous emission was inhibited and the emission intensity decreased. A poly(ethylene glycol) methacrylate-based hydrogel network was used to encapsulate the CCAs and stabilize their crystal-like structure. Within the hydrogel, coupling the photonic bandgap with the radioluminescence of the CCA films led to robust optical systems with tunable emissions. These fully organic, hydrogel-stabilized, radioluminescent CCAs possess mechanochromic tunable optical characteristics with future applications as potentially less toxic X-ray bioimaging materials.

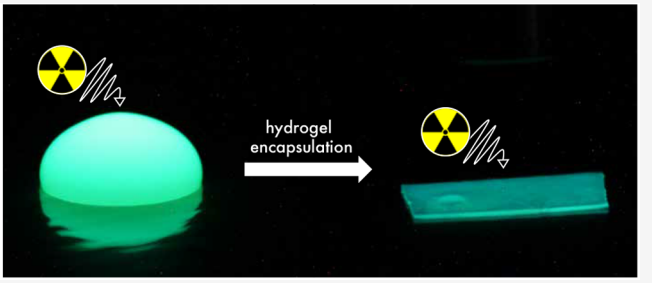

INTRODUCTION

X-ray bioimaging frequently requires toxic, heavy metal contrast agents to produce an image; however, these heavy metals possess various toxicity concerns that limit their practical use.[1−6] Fully organic, radioluminescent nanoparticles utilizing organic scintillators offer a potential route to less toxic X-ray imaging probes.[7] Colloidal nanoparticles are favorable for biological applications due to their high stability in aqueous solutions and ability for modification.[8,9] Pairing fully organic colloidal nanoparticles with organic scintillators may lead to less toxic X-ray imaging probes, as opposed to previously designed nanoparticle probes functionalized with toxic imaging agents.[10−12]

Crystalline colloidal arrays (CCAs) have long been of interest due to their unique optical properties resulting from the long-range ordering of the colloidal nanoparticles.[13] Typically consisting of silica or polymer latex monodisperse nanoparticles, negative surface charges result in Coulombic repulsion forces that cause ordering into a crystalline structure at a sufficiently high particle concentration in aqueous media.[14−16] The negatively charged surfaces of the nanoparticles induce self-assembly into the thermodynamically favored lowest energy state, which in this work is a face-centered-cubic (fcc) crystal structure.[17] This periodic dielectric array results in an appearance mimicking the naturally occurring precious opal. The spatial periodicities result in partial photonic bandgaps in which specific wavelengths of light within the near-visible and visible spectrum are forbidden from propagating through the material.[18] The partial photonic bandgap of the CCA can be adjusted through the near-visible and visible spectrum by changing the interparticle spacing.[13] Because of their adjustable selective light transmission, CCAs can be used as detectors or optical rejection filters.[19] In the efforts to create advanced optical devices, fluorophores are commonly paired with CCAs due to a CCA's distinct ability to modulate fluorophores emission via the partial photonic bandgap.[16,20] When a CCA's partial photonic bandgap (i.e., rejection wavelength) overlaps the emission of an incorporated fluorophore, the emission is suppressed at the rejection wavelength. This well-known phenomenon occurs due to the decreased density of optical modes at the bandgap.[21,22]

In this work, CCAs were functionalized with an organic scintillator (anthracene) to introduce radioluminescent characteristics into the optical system. Introducing an organic scintillator into the CCA system allows for potential applications in various X-ray bioimaging methods such as X-

Received: April 15, 2022
Revised: July 28, 2022
Published: August 9, 2022

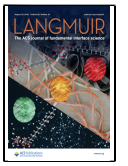

https://doi.org/10.1021/acs.langmuir.2c00977
Langmuir 2022, 38, 10089−10097

ray fluorescence computed tomography (XFCT), which depends on the selective excitation of radioluminescent nanoparticles.[23] The incorporated scintillator can be paired with Förster resonance energy transfer (FRET) pairing fluorescent dyes to control the wavelength at which the CCA emits when excited with ionizing radiation.[18,24] To this end, up to two additional organic emitters (naphthalimide and rhodamine B) were copolymerized in addition to anthracene so that the CCAs emission could span the full visible spectrum via sequential energy transfers.

The crystalline ordering of the liquid CCAs is fragile; there can be a temporary destruction of the array from applied mechanical stress, after which self-assembly may occur once again, or permanent disorder from the introduction of ionic impurities.[13] To combat this fragility and convert the liquid CCAs into a more robust state, the CCAs can be encapsulated in a poly(ethylene glycol) methacrylate (PEGMA)-based hydrogel network. The encapsulating network stabilizes the crystal structure without inhibiting the unique optical characteristics.[13−16] Additionally, converting the fluid optical system into a hydrogel film is favorable for portability and relative ease of handling. The encapsulation in a polymer hydrogel network prevents the destruction of the crystal structure while still allowing for the interparticle spacing to shift by changing the volume of the hydrogel.

Prior work demonstrated the incorporation of a *trans*-stilbene scintillator by physically encapsulating it within a poly(styrene-*co*-propargyl acrylate) CCA;[18] however, the doping process did not yield bright radioluminescent films. To span the visible spectrum, azide-modified FRET pairing emitters were attached to the surface of the nanoparticles post-hydrogel encapsulation by using a copper(I)-catalyzed azide/alkyne cycloaddition "click" reaction, which only allowed a limited amount of the emitters to infiltrate the hydrogel network.[18] In this work, the scintillator and additional emitters were covalently incorporated during the synthesis of the CCA nanoparticles. By employing a copolymerization technique at the initial poly(styrene-*co*-propargyl acrylate) nanoparticle synthesis, a larger quantity of the scintillator and additional emitters could be incorporated within the CCA. In this way, hydrogel-stabilized, fully organic, radioluminescent CCAs with mechanochromic tunable emissions spanning the full visible spectrum were synthesized for potential X-ray bioimaging applications.

EXPERIMENTAL SECTION

Chemical Supplies. Deionized (DI) water was sourced from a Nanopure Diamond System with a resistivity reading of 18.2 MΩ·cm. Reagents and solvents were bought from commercial suppliers (e.g., Sigma-Aldrich or Alfa Aesar). Monomers used in the synthesis of crystalline colloidal arrays (CCAs) were cleaned via filtering through aluminum oxide (Al_2O_3). Mixed-bed ion-exchange resin (BioRad Laboratories, AG 501-X8 resin, 20−50 mesh) beads were mixed with monomers used in the hydrogel network for at least 1 day before using.

Characterization Methods. *Chemical Characterization.* ^{1}H NMR spectra were recorded on a JEOL ECX-300 spectrometer. Chemical shifts for protons are reported in parts per million downfield from tetramethylsilane and are referenced to residual protium in the NMR solvent ($CDCl_3$: δ 7.26 ppm).

Optical Characterization. Reflectance spectra were collected by using an Ocean Optics bifurcated fiber-optic bundle connected to a fiber coupled spectrometer (Ocean Optics USB2000). To irradiate the CCAs encapsulated in hydrogel films, an Amptek Mini-X X-ray unit equipped with a tungsten target was used while operating at 25 kV and 158 μA. Radioluminescence spectra of the hydrogel films were collected via a cooled CCD detector (Synapse, Horiba Jobin Yvon) and a MicroHR monochromator (Horiba Jobin Yvon). The radioluminescence spectra were collected from a slit width of 1 mm over an exposure time between 45 and 90 s, and the signal was collected with a blaze of 500 nm and with a 600 lines mm^{-1} grating. The radioluminescence spectra were collected on the [111] plane of the CCA. Horiba Jobin Yvon SynerJY was the software used to analyze the data collected. The CCA films were dried on top of poly(methyl methacrylate) (PMMA) for data collection because it is optically clear and does not have a signature within the visible light spectrum when irradiated, allowing for observation of the film without interference.

Syntheses. *Synthesis of Anthracen-9-ylmethyl Methacrylate (Anthracene Methyl Methacrylate Derivative, AMMA).* Anthracen-9-ylmethyl methacrylate (AMMA) was synthesized by using a modified method described elsewhere.[25] 9-Anthracenemethanol (4 g, 19.2 mmol) was dissolved in 30 mL of dichloromethane, and then triethylamine was added. The obtained solution was cooled to −5 °C. Methacryloyl chloride was added dropwise to the stirred cooled solution and the obtained mixture was allowed to reach room temperature and was stirred for 6 h (cf. Figure 1). The mixture was

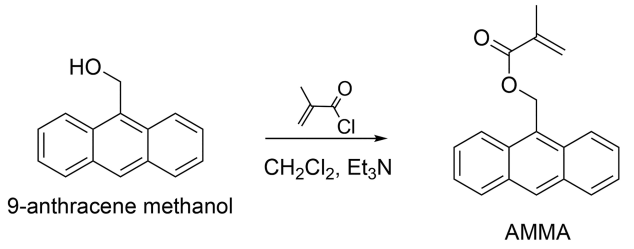

Figure 1. Synthetic scheme to yield anthracen-9-ylmethyl methacrylate (AMMA).

washed with water, and the organic solution was separated and dried with Na_2SO_4, filtered, and evaporated under vacuum. The product was purified by flash column chromatography. Solvent dichloromethane−hexane (1:1), Rf = 0.5. The product was recrystallized from hexane. Yield 3.9 g (73%). ^{1}H NMR (300 MHz, $CDCl_3$, δ, ppm): 1.92 (s, 3H), 5.51 (t, 1H), 6.06 (t, 1H), 6.22 (s, 2H), 7.50 (m, 2H, J = 7.6 Hz, J = 6.9 Hz), 7.58 (m, 2H, J = 7.6 Hz, J = 6.9 Hz), 8.03 (d, 2H, J = 8.9 Hz), 8.38 (d, 2H, J = 8.9 Hz), 8.52 (s, 1H).

Synthesis of 2-(1,3-Dioxo-6-(piperidin-1-yl)-1H-benzo[de]-isoquinolin-2(3H)-yl)ethyl Methacrylate (Naphthalimide Methyl Methacrylate Derivative, NMMA). 2-(2-Hydroxyethyl)-6-(piperidin-1-yl)-1*H*-benzo[*de*]isoquinoline-1,3(2*H*)-dione (**1**) was synthesized according to a previously described method.[26]

2-(1,3-Dioxo-6-(piperidin-1-yl)-1*H*-benzo[*de*]isoquinolin-2(3*H*)-yl)ethyl methacrylate (NMMA) was synthesized by first dissolving (**1**) (0.52 g, 1.6 mmol) and triethylamine (0.21 g, 2.1 mmol) in dry dichloromethane. The solution was cooled to −5 °C. Methacryloyl chloride (0.2 g, 1.92 mmol) was added dropwise to the stirred solution. The obtained mixture was stirred at −5 °C for 30 min, then the cooling bath was removed, and the reaction was stirred at room temperature for an additional 3 h (cf. Figure 2). The mixture was washed with water, and the organic layer was separated, dried with Na_2SO_4, filtered, and evaporated under vacuum at 30 °C. The residue was recrystallized from a methanol/hexane (5/1) mixture, filtered, washed with hexane, and dried. Yield 0.37 g (59%), yellow solid, mp = 136 °C. ^{1}H NMR ($CDCl_3$) δ 1.74 (m, 2H), 1.86 (s, 3H), 1.89 (m, 4H, J = 5.2 Hz), 3.23 (t, 2H, J = 5.2 Hz), 4.48 (d, 2H, J = 4.8 Hz), 4.53 (d, 2H, J = 4.8 Hz), 5.5 (s, 1H), 6.05 (s, 1H), 7.17 (d, 1H, J = 7.9 Hz), 7.68 (d.d, 2H, J = 8.3 Hz, J = 7.2 Hz, J = 1.0 Hz), 8.39 (d.d, 1H, J = 8.3 Hz, J = 1.0 Hz), 8.49 (d, 1H, J = 7.9 Hz), 8.57 (d.d, 1H, J = 7.2 Hz, J = 1.0 Hz). ESI+ Mass (m/z): calculated for $C_{23}H_{24}N_2O_4$ $[M + H]^+$ 393.1736; found 393.1802.

Synthesis of N-(6-(Diethylamino)-9-(2-((2-(methacryloyloxy)-ethoxy)carbonyl)phenyl)-3H-xanthen-3-ylidene)-N-ethylethanami-

https://doi.org/10.1021/acs.langmuir.2c00977
Langmuir 2022, 38, 10089−10097

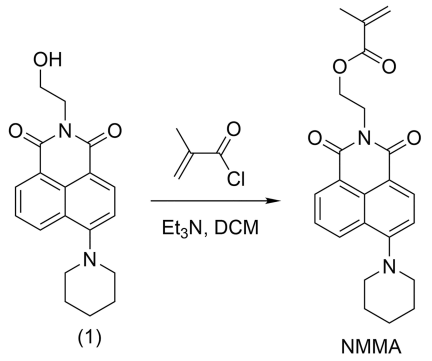

Figure 2. Synthetic scheme to yield 1,3-dioxo-6-(piperidin-1-yl)-1*H*-benzo[*de*]isoquinolin-2(3*H*)-yl)ethyl methacrylate (NMMA).

nium Chloride (Rhodamine B Methyl Methacrylate Derivative, RMMA). *N*-(6-(Diethylamino)-9-(2-((2-(methacryloyloxy)ethoxy)-carbonyl)phenyl)-3*H*-xanthen-3-ylidene)-*N*-ethylethanaminium chloride (RMMA) was synthesized by using a modified method described elsewhere.[27] Rhodamine B acid chloride[28,29] (0.42 g, 0.84 mmol) and 2-hydroxyethyl methacrylate (0.14 g, 1.09 mmol) were dissolved in dry dichloromethane (8 mL). The obtained solution was cooled to 0 °C and degassed with nitrogen. Next, triethylamine (0.13 g, 1.28 mmol) was added into the stirred solution (cf. Figure 3). The cooling was removed, and the mixture was stirred at room temperature for 6 h, washed with water, dried with Na_2SO_4, filtered, and evaporated under reduced pressure at 35 °C. The crude residue was purified by column chromatography on silica. The first solvent dichloromethane/methanol (20/1) washed out impurities and the second solvent dichloromethane/methanol (10/1) washed out a product, Rf = 0.25. Yield 0.33 g (71%), dark-red oil. ^{1}H NMR ($CDCl_3$) δ 1.32 (t, 12H, J = 7.2 Hz), 1.88 (t, 3H, J = 1.3 Hz), 3.64 (q, 8H, J = 7.2 Hz), 4.18 (m, 2H, J = 2.4 Hz), 4.30 (m, 2H, J = 2.4 Hz), 5.55 (t, 1H, J = 1.7 Hz), 6.02 (t, 1H, J = 1.4 Hz), 6.79 (d, 2H, J = 2.4 Hz), 6.91 (d.d, 2H, J = 2.4 Hz, J = 9.3 Hz), 7.05 (d, 2H, J = 9.3 Hz), 7.32 (d.d, 1H, J = 1.0 Hz, J = 7.6 Hz), 7.74 (m, 1H, J = 1.4 Hz, J = 7.6 Hz), 7.83 (m, 1H, J = 1.4 Hz J = 7.6 Hz) 8.29 (d, 1H, J = 1.0 Hz, J = 7.6 Hz).

Synthesis of S_1 CCA Copolymer Nanoparticles. The S_1 CCA nanoparticles described in this paper were synthesized via emulsion copolymerization. The emitter was added such that 0.5% w/w of the anthracene compound (0.067 g of AMMA) was dissolved in purified styrene monomer (14.72 mL or 13.336 g) by sonicating the mixture. DI water (50 mL), 25% of the styrene−AMMA mixture (3.68 mL), and 25% of the propargyl acrylate (0.32 mL) were then added to a four-neck round-bottom flask. The remaining 75% of the previous components were added to a dropping funnel and affixed to one of the necks of the round-bottom flask while a mechanical stirrer, condenser, and thermocouple were attached to the other necks. Stirring was set to 370 rpm, and the contents of the round-bottom flask were purged with nitrogen below the solution level for 40 min. The purge gas was then moved above the solution line, and the temperature was increased to 60 °C. Sodium lauryl sulfate (0.18 mL, 29 mass % in DI water) and divinylbenzene (0.1 mL) were injected into the flask, and the temperature was allowed to stabilize. Once the reaction vessel reached temperature, solutions of sodium hydrogen phosphate (Na_2HPO_4, 0.14 g in 0.8 mL of DI water) and potassium persulfate ($K_2S_2O_8$, 0.14 g in 1.0 mL of DI water) were injected into the round-bottom flask. The temperature was then increased to 71 °C and allowed to stabilize for 20 min. The contents of the dropping funnel were allowed to drip into the reaction vessel at a rate of 1 drop every 2 s. When half of the contents of the dropping funnel had been added, more divinylbenzene (0.24 mL) was injected into the reaction. Once the dropping funnel was emptied, the reaction was allowed to proceed for 2.5 h. The reaction was cooled to 37 °C, and the product was cleaned by gravity filtration. The filtered product was then transferred into dialysis bags (50000 MWCO), dialyzed in a heated DI water bath, and changed frequently until opalescence was observed (ca. 2 weeks). The opalescence indicates the self-assembly of the particles into a CCA. After shaking for 2 days with ion-exchange resin beads in a Nalgene bottle, the CCA was then stored at room temperature. The hydrodynamic diameter of the particles was measured to be 123.4 ± 13.4 nm through dynamic light scattering (DLS, Coulter N4Plus dynamic light scatter). The zeta potential of the CCA was −66.99 ± 1.93 mV and was measured with a ZetaPlus zeta potential analyzer (Brookhaven Instruments Corp.).

Synthesis of S_2 CCA Copolymer Nanoparticles. A similar procedure to that of S_1 was performed to synthesize the S_2 CCA with copolymerized AMMA and the naphthalimide methyl methacrylate derivative (NMMA). At the point in the procedure in which the emitter compound is dissolved in the styrene monomer, 0.3% w/w AMMA and 0.3% w/w NMMA (0.040 g each) were dissolved into the styrene monomer. The remaining procedure was performed the same as previously described. The hydrodynamic size of the particles was 123.6 ± 23.0 nm with a zeta potential of −50.50 ± 1.03 mV.

Synthesis of S_3 CCA Copolymer Nanoparticles. To synthesize the S_3 particles with all three emitters, the same procedure as used in S_2 was performed with the addition of the rhodamine B methyl methacrylate derivative (RMMA), such that 0.3% w/w AMMA, 0.3% w/w NMMA, and 0.3% w/w of RMMA (0.040 g each) were dissolved into the styrene monomer. The hydrodynamic size of the particles was 155.1 ± 14.5 nm with a zeta potential of −70.77 ± 3.40 mV.

Preparation of Glass Cells. The glass cells were prepared according to a previously described method.[18] In brief, the surface of Corning glass slides was modified to be hydrophobic via a treatment using an octadecyltrichlorosilane (OTS) and toluene solution. Two slides were separated with a spacer cut from 2 adhered pieces of Parafilm to form a 2 cm × 1 cm × 250 μm cavity.

Encapsulation in Hydrogel Network. The CCAs were encapsulated in a poly(ethylene glycol) methacrylate (PEGMA)-based hydrogel network via *in situ* photopolymerizations. The hydrogel matrix materials included the PEGMA monomer (MW = 360 g/mol), poly(ethylene glycol) dimethacrylate (PEGDMA) cross-linker (MW = 550 g/mol), and 2,2-diethoxyacetophenone (DEAP) photoinitiator in a 10:1:0.1 ratio, respectively. Typically, 300 μL of CCA in DI water was combined with 55 μL of PEGMA, 5.5 μL of PEGDMA, and 0.6 μL of DEAP. The matrix materials were mixed

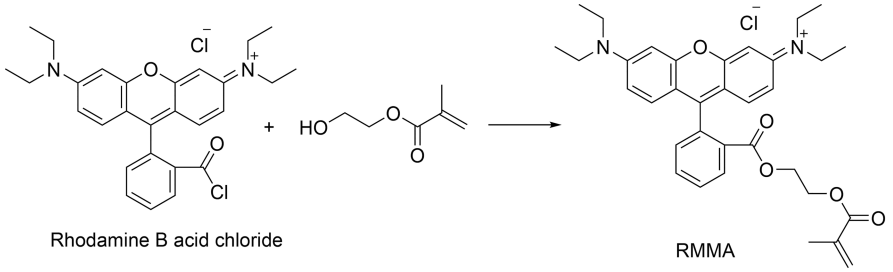

Figure 3. Synthetic scheme to yield *N*-(6-(diethylamino)-9-(2-((2-(methacryloyloxy)ethoxy)carbonyl)phenyl)-3*H*-xanthen-3-ylidene)-*N*-ethylethanaminium chloride (RMMA).

https://doi.org/10.1021/acs.langmuir.2c00977
Langmuir 2022, 38, 10089−10097

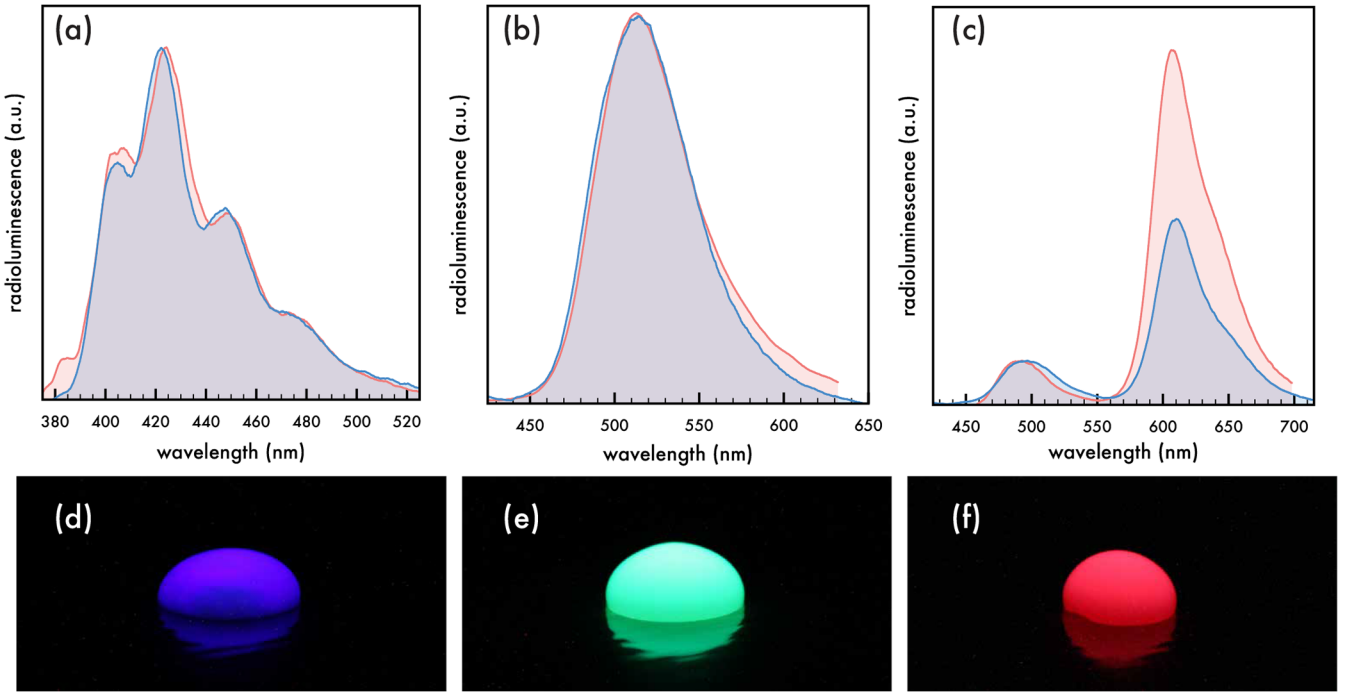

Figure 4. Radioluminescence spectra of liquid CCA systems (red) and hydrogel encapsulated CCAs (blue) with normalized peak heights and rejection wavelengths outside emission range (λ_{rw} > 700 nm): (a) S_1 particles with anthracene derivative (AMMA), (b) S_2 particles with AMMA and naphthalimide derivatives (NMMA), and (c) S_3 particles with AMMA, NMMA, and rhodamine B derivatives (RMMA) with spectra normalized to donor emitter peak height. Optical photographs of (d) S_1, (e) S_2, and (f) S_3 under X-ray irradiation using an AmpTek Mini-X X-ray unit with a tungsten target operating at a tube voltage and amperage of 50 kV and 79 μA, respectively.

with the CCA in a cuvette and shaken until opalescence was observed for the whole mixture, usually overnight. Approximately 60 μL of the CCA−hydrogel mixture was then injected into a glass cell. The cell was exposed to a UV source (ELC-500 light exposure system, Electro-Lite Corporation) for 2 min on each side to photopolymerize the matrix surrounding the CCA. Finally, the hydrogel-encapsulated CCA was removed from the glass cell and stored in DI water.

RESULTS AND DISCUSSION

Figure 4a−c presents the X-ray emission characteristics of the three unique crystalline colloidal arrays (CCAs) synthesized in this effort. Optical photographs of the three liquid CCAs under X-ray irradiation are shown in Figure 4d−f. The particles all employed a base radioluminescent dye that acted as the "pump source" for additional dyes that were covalently incorporated into the particles and were Förster resonance energy transfer (FRET) pairs. Overall, the radioluminescence spectra demonstrated by hydrogel-encapsulated CCA particles matched that of the corresponding liquid CCA system, except for a difference in peak heights for the third emitter combination. The shift in relative peak height in Figure 4c suggests a frustration of the energy transfer mechanism during hydrogel encapsulation.

The first set of particles (S_1) covalently incorporated a derivative of the well-known organic scintillator anthracene, specifically anthracen-9-ylmethyl methacrylate (AMMA). Anthracene is the brightest organic scintillator and emits in the blue region of the visible light spectrum upon irradiation.[30] Following encapsulation in a hydrogel network, the S_1 CCA hydrogel film was excited with X-rays and displayed a radioluminescence spectrum with three peaks at 409, 424, and 449 nm, as well as a shoulder at 480 nm, and is presented in Figure 4a. The three-pronged emission with accompanying shoulder in this region observed via X-ray irradiation is characteristic of anthracene, indicating that the CCA system exhibits the typical radioluminescence of the incorporated scintillator.[30−33]

The second set of particles (S_2) incorporated AMMA and a fluorescent dye, a naphthalimide methyl methacrylate derivative (NMMA), and emitted green light when excited with X-rays. Naphthalimide is a FRET pair with anthracene, which leads to a nonradiative energy transfer between the emitters when both are incorporated into a CCA particle set.[18] The excited AMMA (donor) transfers energy to the NMMA (acceptor). The resulting radioluminescence of the liquid and hydrogel-encapsulated S_2 CCA is shown in Figure 4b; the strong, rounded peak at 511 nm is characteristic of excited naphthalimide.[34] In the emission spectra of the hydrogel-encapsulated S_2, there is no signature of an anthracene emission, suggesting an efficient and total energy transfer from AMMA and NMMA. Utilizing the standard equation for FRET efficiency $E = 1 - \frac{I_D}{I_D + I_A}$, where I_D and I_A are the integrated intensities of the donor and the acceptor, respectively, results in a calculated efficiency of 97.0% for AMMA to NMMA.[35]

The third hydrogel-encapsulated CCA series (S_3) covalently incorporated AMMA, NMMA, and another fluorescent dye, a rhodamine B methyl methacrylate derivative (RMMA). Similar to the previous emitter coupling, rhodamine B is a FRET pair with naphthalimide, such that the excited NMMA (donor) transfers energy to RMMA (acceptor). When all three emitters are incorporated into a CCA system, there is a primarily red light emission with excitation of the system. The radioluminescence of the S_3 hydrogels when irradiated with X-rays was characterized by a short hump with a local maximum at 498 nm and a large peak with a maximum at 611 nm and is

https://doi.org/10.1021/acs.langmuir.2c00977
Langmuir 2022, 38, 10089−10097

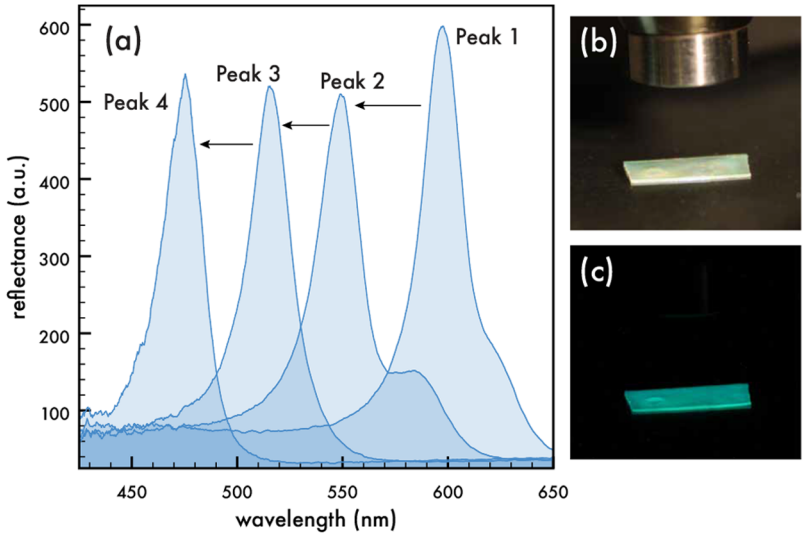

Figure 5. (a) Shift in rejection wavelength of a hydrogel encapsulated CCA film observed as reflectance. The rejection wavelength was blue-shifted by drying the film. Optical photographs of a hydrogel encapsulated S_2 film under (b) white light and (c) X-ray irradiation using an AmpTek Mini-X X-ray unit with a tungsten target operating at a tube voltage and amperage of 50 kV and 79 μA, respectively.

presented in Figure 4c. The short hump is attributed to the emission of NMMA while the large peak is characteristic of rhodamine B emission.[36] This suggests that the energy transfer from the NMMA to the RMMA was not as efficient as the transfer between the first FRET pair. For the S_3 hydrogels, the calculated energy transfer efficiency from AMMA to NMMA was found to be 96.7% and from NMMA to RMMA was 76.8%.

The CCAs exhibit a rejection wavelength at which specific wavelengths of the visible light or near-infrared spectrum are forbidden from propagating throughout the material due to the long-range ordering of the particles.[13,14,37] The rejection wavelength was observed via the reflectance of the material because only photons corresponding to the forbidden wavelength are not transmitted. Any detected emission of the incorporated emitters as a result of excitation from the white light used to collect reflectance data was insignificant compared to observed reflectance data. The rejection wavelength can be estimated by using Bragg's law:

$$\lambda_{rw} = 2n_c d_{hkl} \sin(\theta) \quad (1)$$

where λ_{rw} is the rejection wavelength, n_c is the refractive index of the composite system, d_{hkl} is the interplanar spacing of the scattering planes, and θ is the angle of incidence.[14,38] The rejection wavelength of the CCA particles is directly proportional to the interplanar spacing of the CCA at a set angle of incidence. These crystals exhibit mechanochromism, where a mechanical change in the interparticle spacing, and corresponding interplanar spacings, results in a change in the rejection wavelength supported by the crystal. For example, mechanochromism can be achieved in these arrays by diluting a liquid CCA with deionized water. The dilution will lower the concentration of the particles, allowing the particles to undergo an affine transformation to larger interparticle spacings. Neglecting changes in the refractive index of the system, the increased interparticle distance will result in a bathochromic shift of the rejection wavelength.

Similarly with a hydrogel-encapsulated CCA, the CCA film can be dried in air and rehydrated to effectively deswell and reswell the film and manipulate the interparticle spacing. As the hydrogel network shrinks as it is drying out, the CCA particles are brought closer together, resulting in a hypsochromic shift of the rejection wavelength. DI water added to the partially dehydrated film will be absorbed, and the film will expand to its original dimensions, red-shifting the rejection wavelength back toward its initial position. Figure 5a presents a bathochromic shift of the rejection wavelength for a hydrogel-encapsulated CCA as it is slowly allowed to dry out. The fully hydrated film initially has a rejection wavelength of 598 nm (peak 1), which slowly shifts to 475 nm (peak 4), passing through intermediate wavelengths, by drying the CCA film on a PMMA substrate over the course of 2 h in a 23 °C 40% RH room. Figures 5b and 5c present optical photographs of an S_2 film under white light and X-ray irradiation, respectively.

For the CCA films used in this work, the refractive index (n_c) is assumed to remain constant at 1.368, the plane of interest is the (111) plane, and the angle of incidence is maintained at 90°.[13] Approximated with Bragg's law, Table 1 contains interparticle spacing (d_{111}) for each reflectance peak observed in Figure 5a. By use of these values, the lattice parameter for an fcc structure was calculated by $a_c = \sqrt{3}\, d_{111}$, and the nearest-neighbor distance was found with $a = a_c/\sqrt{2}$. By shifting the rejection wavelength from 598 to 475 nm, a ca. 123 nm total shift, the nearest-neighbor distance was decreased by 20.6%. The change in the dimensions of the gel in going from peak 1 to peak 4 translates to ca. 50% decrease in the lattice cell volume.

Table 1. Change in Lattice Parameters for Hydrogel Encapsulated CCA as the Rejection Wavelength Is Blue-Shifted (Cf. Figure 5)

	peak 1	peak 2	peak 3	peak 4
n_c	1.368	1.368	1.368	1.368
λ (nm)	598	549	515	475
d_{111} (nm)	218.6	200.7	188.2	173.6
a_c (nm)	378.6	347.5	326.0	300.7
a (nm)	267.7	245.8	230.5	212.6

https://doi.org/10.1021/acs.langmuir.2c00977
Langmuir 2022, 38, 10089−10097

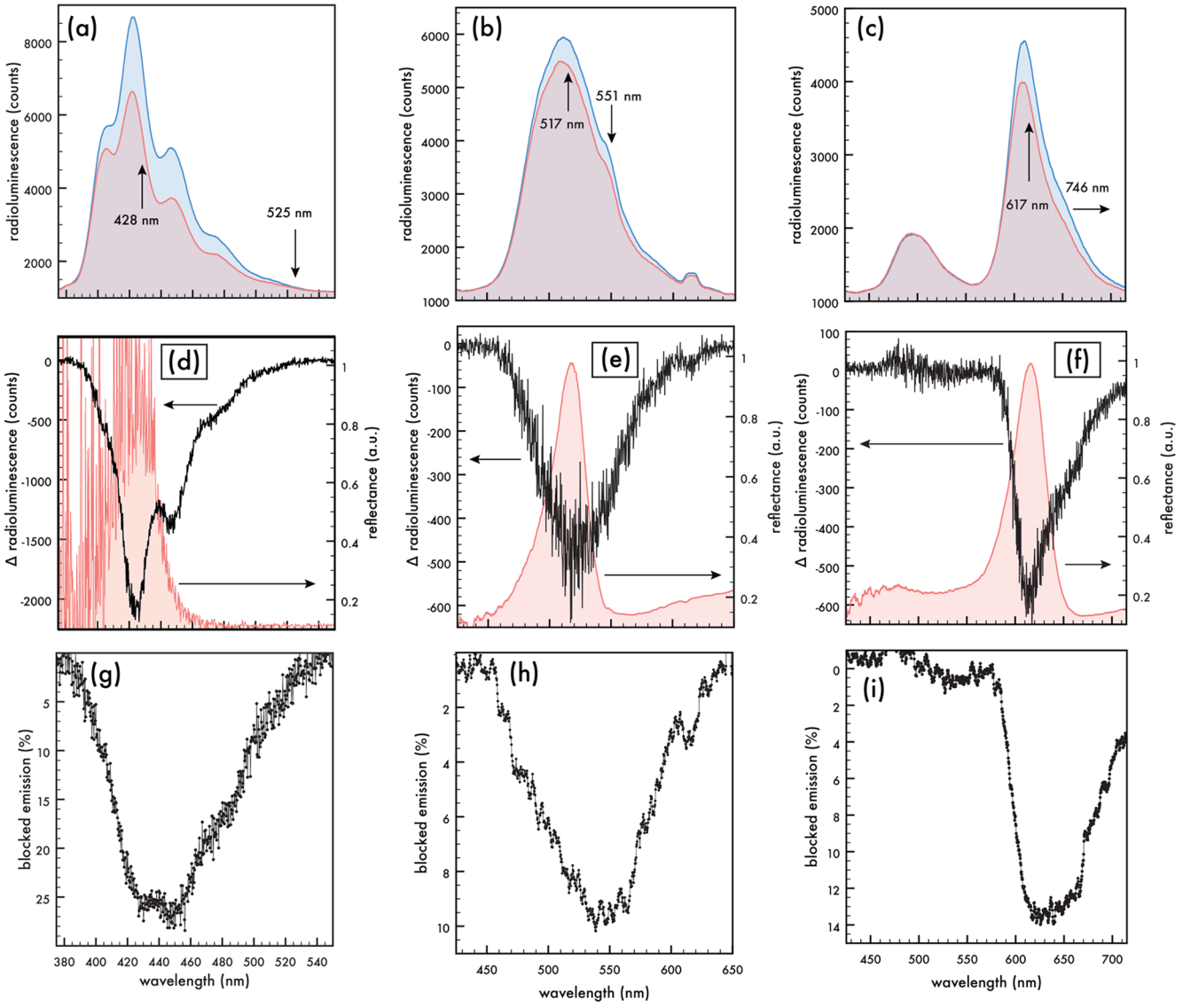

Figure 6. Emission characteristics of hydrogel-encapsulated CCAs: (a) radioluminescence of S_1 gel with rejection wavelength at 428 and 525 nm, (b) radioluminescence of S_2 gel with rejection wavelength at 517 and 551 nm, and (c) radioluminescence of S_3 gel with rejection wavelength at 617 and 746 nm. The difference between the emission spectra of (d) S_1, (e) S_2, and (f) S_3 when the rejection wavelength (1) overlapped the emission peak and (2) was outside the emission range. In addition, (d), (e), and (f) present the reflection spectra when the rejection wavelength coincided with the peak of emission of the dyes. Percentage change in radioluminescence of the (g) S_1 hydrogel film with rejection wavelength at 428 and 525 nm, (h) S_2 hydrogel film with rejection wavelength at 517 and 551 nm, and (i) S_3 hydrogel film with rejection wavelength at 617 and 746 nm.

According to FRET theory, the distance required for an efficient energy transfer is generally in the range 1−10 nm.[39] The estimated interparticle spacing within the CCAs presented in Table 1 is at least 20−30 times greater than typical FRET distances and eliminates the possibility for an interparticle FRET exchange, instead suggesting there is only nonradiative energy transfer at an intraparticle level. Similarly, as collected radioluminescence spectra of the films did not significantly vary based on volume changes of the system during swelling/deswelling studies, it was concluded there was insignificant radiative interparticle energy exchange.

Coupling the Rejection Wavelength with the Emission. As the partial photonic bandgap created by the periodicity of the crystalline colloidal array prevents wavelengths within the stopband from transmitting through the crystal, a decrease in radioluminescence is expected to be observed if the rejection wavelength is shifted to overlap with the emission of a targeted emitter.[18,20]

For each set of CCA particles encapsulated in a hydrogel, emission spectra were compared before and after shifting the rejection wavelength to overlap the peak emission of the dominant fluorophore within the three types of particles and is presented in Figure 6a−c. In each case, an overall decrease in emission of the dominant emitter was observed with varying levels of suppression. Notably, Figure 6c indicates that when the rejection wavelength is centered at 617 nm, only the emission of RMMA (peak at 611 nm) in the S_3 film was affected while NMMA emission remained largely unchanged. This suggests that, in this case, the rejection wavelength causes only a local suppression of the radioluminescence.

The rejection wavelength of the S_1 gel was shifted from 528 to 428 nm, and the total observed radioluminescence

https://doi.org/10.1021/acs.langmuir.2c00977
Langmuir 2022, 38, 10089−10097

decreased by 26%. The smallest suppression observed for a targeted emitter was a 10% decrease in the NMMA emission in the S_2 gels with a rejection wavelength shift from 551 to 517 nm. For a liquid CCA system with a single crystal, a distinct drop in the emission is expected as previously demonstrated.[7] However, studies have shown that defects present in the crystalline array of particles affect the optical characteristics in multiple ways, such as broadening the bandwidth or lessening the intensity of the bandgap.[40,41] Furthermore, a previous experiment suggests that encapsulating the CCA particles in a polymerized hydrogel network inherently introduces defects to the system.[13] The defects incorporated into the CCAs during photopolymerization *in situ* with the hydrogel network result in multiple crystals within one film, all with slightly different interparticle spacing. This, coupled with nonuniform evaporation of the hydrogel films in air as the edges dry out sooner, results in films with nonuniform photonic bandgaps. The presence of defects is confirmed by comparing the bandwidths measured by the full width at half-maximum (FWHM) of the reflectance peaks. The narrowest bandwidth for a CCA film in this work was ca. 34 nm, observed for an S_1 CCA film with a rejection wavelength $\lambda > 500$ nm. This is more than double that of the ca. 14 nm bandwidth observed for a monolithic polymerized CCA previously fabricated.[42] Additionally, the variance of the rejection wavelength across the films causes the radioluminescence suppression to occur at more than one single wavelength, so a general reduction in the emission is observed instead of a sharp decrease.

The difference between the two collected emission spectra (cf. Figure 6d−f) is expected to largely center around the reflectance observed when the rejection wavelength has been shifted to overlap the emission. Although for each film the reflection was within the region in which a decreased emission occurred, the difference curves were broader than the reflectance or were not the expected shape. It is supposed that the broadness of the radioluminescence suppression is caused by previously discussed defects in the crystal structure of the CCAs within the films. The shape of the difference curve for the S_1 film (cf. Figure 6d) appears to have two separate regions of emission suppression at 424 and 447 nm. However, these peaks mirror two of the three peaks of AMMA emission nearly exactly, and the shape of the difference curve for the S_3 film (cf. Figure 6f) also mirrors the initial emission of RMMA. When the percentage of emission that is blocked is considered for each point (cf. Figure 6g−i), a singular depression is observed for each of the films. Each observed rejection wavelength is located within these depressions, while the broadness of the depression corresponds to the relative amount of defects within the crystalline structure in the films. Because the emission suppression was so shallow and over the widest range, the S_2 film is suggested to have the most defects within its structure. The partial bandgap had the highest intensity in the S_1 gel, with a maximum blocked emission of ca. 27%, while the range of rejection wavelengths was narrowest in the S_3 film.

CONCLUSION

This work demonstrated the effect of a rejection wavelength on the exhibited radioluminescence of a crystalline colloidal array (CCA) encapsulated in a poly(ethylene glycol) methacrylate (PEGMA)-based hydrogel network. The CCA films presented were able to emit across the entire visible light spectrum by covalently incorporating fully organic emitters into the CCA nanoparticles. The emitters used were a scintillator and two fluorescent dyes; the scintillator was an anthracene derivative, and the dyes were naphthalimide and rhodamine B derivatives. Three different combinations of the emitters were used in this work to emit certain colors of light upon irradiation: blue light from S_1, green light from S_2, and red light from S_3. The anthracene component absorbs X-rays and subsequently either emits blue light or transfers the energy in the presence of the naphthalimide component, which then either emits green light or transfers energy to the rhodamine B component. The rejection wavelength resultant from the long-range ordering of the monodisperse poly(styrene-*co*-propargyl acrylate)-based nanoparticles forming the CCA served as a tool to tailor the radioluminescence by suppressing the propagation of photons at specific wavelengths of light in the visible spectrum, thus reducing the emission at those same wavelengths. The position of the rejection wavelength was controlled via the volume of the hydrogel, which related to the interparticle spacing of the CCA. The presence of defects in the crystalline array affected the range and intensity of radioluminescence suppression. Ultimately, the emission of the CCA films was tuned by coupling the emitters incorporated with the partial bandgap.

AUTHOR INFORMATION

Corresponding Author

Stephen H. Foulger − *Center for Optical Materials Science and Engineering Technologies (COMSET), Clemson University, Anderson, South Carolina 29625, United States; Department of Materials Science and Engineering and Department of Bioengineering, Clemson University, Clemson, South Carolina 29634, United States;* orcid.org/0000-0002-4221-2154; Email: foulger@clemson.edu

Authors

Sarah Mell − *Center for Optical Materials Science and Engineering Technologies (COMSET), Clemson University, Anderson, South Carolina 29625, United States; Department of Materials Science and Engineering, Clemson University, Clemson, South Carolina 29634, United States*

Haley W. Jones − *Center for Optical Materials Science and Engineering Technologies (COMSET), Clemson University, Anderson, South Carolina 29625, United States; Department of Materials Science and Engineering, Clemson University, Clemson, South Carolina 29634, United States*

Yuriy P. Bandera − *Center for Optical Materials Science and Engineering Technologies (COMSET), Clemson University, Anderson, South Carolina 29625, United States; Department of Materials Science and Engineering, Clemson University, Clemson, South Carolina 29634, United States*

Complete contact information is available at: https://pubs.acs.org/10.1021/acs.langmuir.2c00977

Notes

The authors declare no competing financial interest.

ACKNOWLEDGMENTS

The authors thank the Gregg-Graniteville Foundation and the National Science Foundation (OIA-1632881) for financial support. The authors also thank the National Institutes of Health (S10 OD021758-01A1) for financial support relating to mass spectroscopy.

REFERENCES

(1) Paik, T.; Gordon, T. R.; Prantner, A. M.; Yun, H.; Murray, C. B. Designing tripodal and triangular gadolinium oxide nanoplates and self-assembled nanofibrils as potential multimodal bioimaging probes. *ACS Nano* **2013**, *7*, 2850−2859.

(2) Carpenter, C. M.; Sun, C.; Pratx, G.; Rao, R.; Xing, L. Hybrid x-ray/optical luminescence imaging: Characterization of experimental conditions. *Med. Phys.* **2010**, *37*, 4011−4018.

(3) Guo, T.; Lin, Y.; Zhang, W. J.; Hong, J. S.; Lin, R. H.; Wu, X. P.; Li, J.; Lu, C. H.; Yang, H. H. High-efficiency x-ray luminescence in Eu3+-activated tungstate nanoprobes for optical imaging through energy transfer sensitization. *Nanoscale* **2018**, *10*, 1607−1612.

(4) Sudheendra, L.; Das, G. K.; Li, C. Q.; Stark, D.; Cena, J.; Cherry, S.; Kennedy, I. M. NaGdF4:Eu3+ nanoparticles for enhanced x-ray excited optical imaging. *Chem. Mater.* **2014**, *26*, 1881−1888.

(5) Li, X. L.; Xue, Z. L.; Jiang, M. Y.; Li, Y. B.; Zeng, S. J.; Liu, H. R. Soft x-ray activated NaYF4:Gd/Tb scintillating nanorods for in vivo dual-modal x-ray/x-ray-induced optical bioimaging. *Nanoscale* **2018**, *10*, 342−350.

(6) Lee, N.; Choi, S. H.; Hyeon, T. Nano-sized CT contrast agents. *Adv. Mater.* **2013**, *25*, 2641−2660.

(7) Burdette, M. K.; Bandera, Y. P.; Gray, G. M.; Foulger, S. H. Dynamic emission tuning of x-ray radioluminescent crystalline colloidal arrays: Coupling the optical stop band with sequential forster resonance energy transfers. *Adv. Opt. Mater.* **2019**, *7*, 1801142.

(8) Reisch, A.; Klymchenko, A. S. Fluorescent polymer nanoparticles based on dyes: Seeking brighter tools for bioimaging. *Small* **2016**, *12*, 1968−1992.

(9) Zheng, C.; Zheng, M.; Gong, P.; Jia, D.; Zhang, P.; Shi, B.; Sheng, Z.; Ma, Y.; Cai, L. Indocyanine green-loaded biodegradable tumor targeting nanoprobes for in vitro and in vivo imaging. *Biomaterials* **2012**, *33*, 5603−5609.

(10) Peuster, M.; Fink, C.; von Schnakenburg, C. Biocompatibility of corroding tungsten coils: in vitro assessment of degradation kinetics and cytotoxicity on human cells. *Biomaterials* **2003**, *24*, 4057−4061.

(11) Haley, T. J.; Flesher, A. M.; Komesu, N.; Upham, H. C.; Cawthorne, J.; Mavis, L. Pharmacology and toxicology of terbium, thulium, and ytterbium chlorides. *Toxicol. Appl. Pharmacol.* **1963**, *5*, 427−436.

(12) Zhou, G. Q.; Li, Y. F.; Ma, Y. Y.; Liu, Z.; Cao, L. L.; Wang, D.; Liu, S. D.; Xu, W. S.; Wang, W. Y. Size-dependent cytotoxicity of yttrium oxide nanoparticles on primary osteoblasts in vitro. *J. Nanoparticle Res.* **2016**, *18*, 135.

(13) Foulger, S. H.; Jiang, P.; Ying, Y.; Lattam, A.; Smith, D., Jr.; Ballato, J. Photonic bandgap composites. *Adv. Mater.* **2001**, *13*, 1898−1901.

(14) Asher, S.; Holtz, J.; Liu, L.; Wu, Z. Self-assembly motif for creating submicron periodic materials. Polymerized crystalline colloidal arrays. *J. Am. Chem. Soc.* **1994**, *116*, 4997−4998.

(15) Holtz, J. H.; Asher, S. Polymerized colloidal crystal hydrogel films as intelligent chemical sensing materials. *Nature* **1997**, *389*, 829−832.

(16) Evanoff, D., Jr.; Hayes, S.; Ying, Y.; Shim, G. H.; Lawrence, J. R.; Carroll, J. B.; Roeder, R. D.; Houchins, J. M.; Huebner, C. F.; Foulger, S. H. Functionalization of crystalline colloidal arrays through click chemistry. *Adv. Mater.* **2007**, *19*, 3507−3512.

(17) Monovoukas, Y.; Gast, A. P. The experimental phase diagram of charged colloidal suspensions. *J. Colloid Interface Sci.* **1989**, *128*, 533−548.

(18) Burdette, M. K.; Jones, H. W.; Bandera, Y.; Foulger, S. H. X-ray radioluminescent hydrogel stabilized crystalline colloidal arrays. *Opt. Mater. Express* **2019**, *9*, 1416−1429.

(19) Yetisen, A. K.; Butt, H.; Volpatti, L. R.; Pavlichenko, I.; Humar, M.; Kwok, S. J. J.; Koo, H.; Kim, K. S.; Naydenova, I.; Khademhosseini, A.; Hahn, S. K.; Yun, S. H. Photonic hydrogel sensors. *Biotechnol. Adv.* **2016**, *34*, 250−271.

(20) Lawrence, J. R.; Shim, G. H.; Jiang, P.; Han, M. G.; Ying, Y.; Foulger, S. H. Dynamic tuning of photoluminescent dyes in crystalline colloidal arrays. *Adv. Mater.* **2005**, *17*, 2344−2349.

(21) Lodahl, P.; van Driel, A. F.; Nikolaev, I. S.; Irman, A.; Overgaag, K.; Vanmaekelbergh, D.; Vos, W. L. Controlling the dynamics of spontaneous emission from quantum dots by photonic crystals. *Nature* **2004**, *430*, 654−657.

(22) Fujita, M.; Takahashi, S.; Tanaka, Y.; Asano, T.; Noda, S. Simultaneous inhibition and redistribution of spontaneous light emission in photonic crystals. *Science* **2005**, *308*, 1296−1298.

(23) Kuang, Y.; Pratx, G.; Bazalova, M.; Meng, B. W.; Qian, J. G.; Xing, L. First demonstration of multiplexed x-ray fluorescence computed tomography (XFCT) imaging. *IEEE Trans. Med. Imaging* **2013**, *32*, 262−267.

(24) Eftekhari, E.; Cole, I. S.; Li, Q. The effect of fluorophore incorporation on fluorescence enhancement in colloidal photonic crystals. *Phys. Chem. Chem. Phys.* **2016**, *18*, 1743−1749.

(25) Bilir, C.; Erdogan, T.; Odabas, S.; Unveren, E. Novel partially fluorinated graft block copolymer ionomer as potential proton exchange membrane material. *Polymer* **2016**, *95*, 91−101.

(26) Chereddy, N. R.; Thennarasu, S.; Mandal, A. B. A highly selective and efficient single molecular FRET based sensor for ratiometric detection of Fe3+ ions. *Analyst* **2013**, *138*, 1334−1337.

(27) Song, J.; Duan, B.; Wang, C.; Zhou, J.; Pu, L.; Fang, Z.; Wang, P.; Lim, T. T.; Duan, H. SERS-encoded nanogapped plasmonic nanoparticles: growth of metallic nanoshell by templating redox-active polymer brushes. *J. Am. Chem. Soc.* **2014**, *136*, 6838−6841.

(28) Morales-Sanfrutos, J.; Lopez-Jaramillo, J.; Ortega-Munoz, M.; Megia-Fernandez, A.; Perez-Balderas, F.; Hernandez-Mateo, F.; Santoyo-Gonzalez, F. Vinyl sulfone: A versatile function for simple bioconjugation and immobilization. *Org. Biomol. Chem.* **2010**, *8*, 667−675.

(29) Xu, M.; Liu, L.; Yan, Q. Allosterically activated protein self-assembly for the construction of helical microfilaments with tunable helicity. *Angew. Chem., Int. Ed. Engl.* **2018**, *57*, 5029−5032.

(30) Knoll, G. F. *Radiation Detection and Measurement*; John Wiley and Sons: 2010.

(31) Birks, J. B. *The Theory and Practice of Scintillation Counting*, 1st ed.; Pergamon Press Ltd.: 1964.

(32) Chandross, E. A.; Ferguson, J.; McRae, E. G. Absorption and emission spectra of anthracene dimers. *J. Chem. Phys.* **1966**, *45*, 3546−3553.

(33) Sidman, J. W. Electronic and vibrational states of anthracene. *J. Chem. Phys.* **1956**, *25*, 115−121.

(34) Ren, J.; Zhao, X. L.; Wang, Q. C.; Ku, C. F.; Qu, D. H.; Chang, C. P.; Tian, H. Synthesis and fluorescence properties of novel co-facial folded naphthalimide dimers. *Dyes Pigm* **2005**, *64*, 179−186.

(35) Blum, C.; Zijlstra, N.; Lagendijk, A.; Wubs, M.; Mosk, A. P.; Subramaniam, V.; Vos, W. L. Nanophotonic control of the forster resonance energy transfer efficiency. *Phys. Rev. Lett.* **2012**, *109*, 203601.

(36) Kedia, S.; Sinha, S. Energy transfer from Rhodamine-B to Oxazine-170 in the presence of photonic stop band. *Opt. Commun.* **2015**, *339*, 41−46.

(37) Jethmalani, J. M.; Ford, W. T. Diffraction of visible light by ordered monodisperse silica-poly(methyl acrylate) composite films. *Chem. Mater.* **1996**, *8*, 2138−2146.

(38) Rundquist, P.; Photinos, P.; Jagannathan, S.; Asher, S. Dynamical Bragg diffraction from crystalline colloidal arrays. *J. Chem. Phys.* **1989**, *91*, 4932−4941.

(39) Wu, W. B.; Wang, M. L.; Sun, Y. M.; Huang, W.; Cui, Y. P.; Xu, C. X. Fluorescent polystyrene microspheres with large Stokes shift by fluorescence resonance energy transfer. *J. Phys. Chem. Solids* **2008**, *69*, 76−82.

(40) Vlasov, Y. A.; Astratov, V. N.; Baryshev, A. V.; Kaplyanskii, A. A.; Karimov, O. Z.; Limonov, M. F. Manifestation of intrinsic defects in optical properties of self-organized opal photonic crystals. *Phys. Rev. E* **2000**, *61*, 5784−5793.

(41) Ye, Y.; LeBlanc, F.; Haché, A.; Truong, V. Self-assembling three-dimensional colloidal photonic crystal structure with high crystalline quality. *Appl. Phys. Lett.* **2001**, *78*, 52−54.

https://doi.org/10.1021/acs.langmuir.2c00977
Langmuir 2022, 38, 10089−10097

(42) Foulger, S. H.; Jiang, P.; Lattam, A. C.; Smith, D. W.; Ballato, J. Mechanochromic response of poly (ethylene glycol) methacrylate hydrogel encapsulated crystalline colloidal arrays. *Langmuir* **2001**, *17*, 6023−6026.

https://doi.org/10.1021/acs.langmuir.2c00977
Langmuir 2022, 38, 10089−10097